SIAM J. SCI. COMPUT.
Vol. 41, No. 1, pp. B93–B113

A FINITE VOLUME SCHEME PRESERVING MAXIMUM PRINCIPLE FOR THE SYSTEM OF RADIATION DIFFUSION EQUATIONS WITH THREE-TEMPERATURE*

YUNLONG YU†, XINGDING CHEN‡, AND GUANGWEI YUAN†

Abstract. We propose a cell-centered nonlinear finite volume scheme for the nonequilibrium three-temperature equations, where both the Dirichlet and Neumann boundary conditions are considered, and prove that the discrete solutions of the scheme satisfy the discrete maximum principle. In the construction of the flux we use the nonlinear combination of two single fluxes and the interpolation technique for the auxiliary unknowns. Some new interpolation methods are introduced, especially when the Neumann boundary condition is considered. Based on the bounded estimation of the discrete solution, we prove that there exists at least a solution for our scheme by using the Brouwer's fixed point theorem. Numerical results show that our scheme has second-order accuracy and good conservation and can preserve the discrete maximum principle.

Key words. discrete maximum principle, finite volume scheme, existence of a solution, radiation diffusion equation with three-temperature

AMS subject classifications. 65M08, 65M22

DOI. 10.1137/18M1167024

1. Introduction.

Radiation transport in astrophysical phenomena and inertial confinement fusion is often modeled by the diffusion approximation. When the radiation field is not in the thermodynamic equilibrium, a coupled system of nonequilibrium diffusion equations is used to simulate the radiation transport, including both radiation diffusion and heat conduction in the material. In some practical problems, the thermal relaxation time scales between the electrons and ions are comparable to the typical time scales of interest, and the electrons and ions may have different temperatures. Therefore, it is necessary to describe the process by nonequilibrium three-temperature (for electron, ion, and photon, respectively) diffusion equations. These nonequilibrium equations are highly nonlinear and tightly coupled and exhibit multiple time and space scales. So, it is a very challenging problem to construct a numerical algorithm with high accuracy and efficiency.

The maximum principle is an important feature of the equilibrium diffusion equation. Under some additional nonnegativity assumptions on the exchange coefficients, it is also satisfied by the nonequilibrium diffusion equations; see [1] or [2]. As we know, the discrete maximum principle (DMP) ensures the nonnegativity and eliminates nonphysical oscillations of numerical solutions. Hence, it is a desirable property for the numerical schemes. In solving the Lagrangian radiation-hydrodynamic problems of complicated flow, distorted meshes are formed on which the coupled system of radiation and material energy equations are solved. It is more difficult to develop an

*Submitted to the journal's Computational Methods in Science and Engineering section January 25, 2018; accepted for publication (in revised form) December 5, 2018; published electronically February 5, 2019.

http://www.siam.org/journals/sisc/41-1/M116702.html

Funding: This work was supported by the National Natural Science Foundation of China through grants 11571048, 11671049, and 11401015.

†Institute of Applied Physics and Computational Mathematics, Beijing, 100088 (yu_yunlong@iapcm.ac.cn, yuan_guangwei@iapcm.ac.cn).

‡College of Science, Beijing Technology and Business University, Beijing (chenxd@th.btbu.edu.cn).

accurate discretization method that satisfies the DMP for solving the coupled system.

In past decades, many authors have addressed this issue and proposed different schemes preserving DMP for the diffusion equations [3, 4, 5, 6, 7, 8, 9, 10, 11, 12, 13, 14, 15, 16, 17, 18]. Most of them focused on solving the single diffusion equation [3, 4, 5, 6, 7, 8, 9, 10, 11, 12, 13]. Under restrictive assumptions on computation meshes, a second-order scheme preserving DMP is proposed by nonlinear combination of multipoint fluxes in [3] for diffusion equations with isotropic coefficients. In [4] and [5], the nonlinear combination idea of [3] is extended to construct the schemes satisfying DMP on generic meshes. Although the way of choosing auxiliary points is different in [4] and [5], both the resulting schemes attain second-order accuracy. Moreover, the existence and the convergence for the scheme are proved in [4]. A scheme with DMP and minimal stencil is designed in [6] by using only cell-centered unknowns in the construction of the normal fluxes. Some new schemes satisfying DMP are constructed by devising a nonlinear modification of the existing linear schemes in [7, 8, 9]. A finite volume scheme preserving DMP on general polygonal mesh is developed in [13], where two kinds of combination of the fluxes are successively devised on each interior edge, and a new interpolation method is used to calculate auxiliary unknowns. An overview of finite volume methods for diffusion equations is given in [10], with special attention to the coercivity and DMP of the schemes.

Now we describe briefly some works on numerical methods for solving nonequilibrium diffusion equations on distorted meshes; see [14, 15, 16, 17, 18]. In [14], a monotone finite volume scheme on distorted meshes is constructed for multimaterial nonequilibrium radiation diffusion problems. It is proved that this scheme preserves positivity on various distorted meshes. A Picard–Newton iterative method with time step controls is designed in [15]. A new tailored finite point method scheme is presented in [16], and it is proved it is monotone under the condition that the time step is sufficiently small. In [17, 18], the monotone scheme in [14] is adopted in solving the three-temperature (3T) radiation diffusion problem, and an extensive test of the scheme is performed for various axis-symmetric radiation-hydrodynamic problems.

It is worth pointing out that all of these schemes mentioned above can preserve only monotonicity, but not the DMP. The monotonicity refers to being nonnegativity maintaining, which is a special case of the DMP. In this paper, we will extend the scheme of the single diffusion equation in [13] and construct a new nonlinear finite volume scheme for the nonequilibrium 3T equations, which satisfies the DMP. Furthermore, the existence of a discrete solution for our nonlinear scheme is proved. The main idea of constructing the scheme is similar to that in [13]. However, there are some differences between them. The scheme in [13] is focused on the single diffusion equation with Dirichlet boundary condition. Our aim here is to accurately solve the coupled 3T equations, in which the thermal exchange terms must be treated. Moreover, we consider both the Dirichlet and Neumann boundary conditions, since the practical problems are often modeled with heat flow boundary. Some new interpolation methods are introduced to calculate these auxiliary unknowns near the boundary of the domain, while the Neumann boundary condition is adopted. Finally, the proof of the existence of a solution of our scheme is somewhat different from the previous works. Note that it is possible to extend the scheme preserving DMP to three-dimensional cases by using the methods in [20, 21].

The rest of this paper is organized as follows. In section 2, we describe the construction of the nonlinear scheme for the 3T diffusions equations. In section 3, we present the method to calculate auxiliary unknowns near the domain boundary.

In section 4, the proof of main theoretical results is given for our nonlinear scheme, which includes both the DMP and the existence of the discrete solution. Numerical results are presented to test the conservation, the accuracy, and the DMP in section 5. Some conclusions are given in section 6.

2. Construction of scheme.

2.1. The model problem and notation. We are interesting in designing a finite volume scheme satisfying the DMP for the following system of 3T diffusion equations:

$$\rho c_{ve}\frac{\partial u_e}{\partial t} - \nabla\cdot(\kappa_e\nabla u_e) = \omega_{ei}(u_i-u_e)+\omega_{er}(u_r-u_e)+W_e \quad \text{in}\Omega\backslash\Gamma, \tag{1}$$

$$\rho c_{vi}\frac{\partial u_i}{\partial t} - \nabla\cdot(\kappa_i\nabla u_i) = \omega_{ei}(u_e-u_i)+W_i \quad \text{in } \Omega\backslash\Gamma, \tag{2}$$

$$\rho c_{vr}\frac{\partial u_r}{\partial t} - \nabla\cdot(\kappa_r\nabla u_r) = \omega_{er}(u_e-u_r) \quad \text{in } \Omega\backslash\Gamma, \tag{3}$$

where $t>0$ and Ω is a bounded polygonal domain in R^2, ρ is the material density, Γ is the material interface, $\mathbf{u}=(u_e,u_i,u_r)$ denotes the electron, ion, and photon temperatures, respectively, $\kappa_\alpha=\kappa_\alpha(u_\alpha)$ and $c_{v\alpha}=c_{v\alpha}(u_\alpha)$ are the diffusion coefficients and the heat capacity of the particle α, $\alpha\in\{e,i,r\}$, all the temperatures u_α and normal fluxes $\kappa_\alpha\frac{\partial u_\alpha}{\partial\vec{n}}$ are continuous across the material interface Γ, $\alpha\in\{e,i,r\}$, $\vec{n}$ is the unit normal vector of Γ, $\omega_{ei}=\omega_{ei}(\mathbf{u})$ is the thermal exchange coefficient between electrons and ions, and $\omega_{er}=\omega_{er}(\mathbf{u})$ is the one between electrons and photons. All of these coefficients are assumed to be positive. W_e and W_i are source terms.

The initial condition is

$$u_\alpha(\mathbf{x},0)=\varphi_\alpha(\mathbf{x}),\alpha\in\{e,i,r\}. \tag{4}$$

We consider two kinds of boundary conditions: the Dirichlet boundary condition

$$u_\alpha(\mathbf{x},t)|_{\partial\Omega}=g_\alpha(\mathbf{x},t) \tag{5}$$

and the Neumann boundary condition

$$\kappa_\alpha\nabla u_\alpha(\mathbf{x},t)\cdot\vec{n}|_{\partial\Omega}=g_\alpha(\mathbf{x},t),\alpha\in\{e,i,r\}. \tag{6}$$

We use a mesh $\mathcal{T}$ to partition the domain Ω. The mesh $\mathcal{T}$ consists of polygonal cells K, i.e., $\overline{\Omega}=\bigcup_{K\in\mathcal{T}}\overline{K}$, ∂K is the boundary of K. Set $h=\sup_{K\in\mathcal{T}}\text{diam}(K)$, where $\text{diam}(K)$ is the diameter of K. The area of K is denoted by S_K. The central point in K is denoted by x_K, which is usually taken to be the barycenter.

Let $\mathcal{A}$ be the set of the edges of all the cells. Denote $\mathcal{A}=\mathcal{A}_{int}\bigcup\mathcal{A}_{ext}$, where $\mathcal{A}_{ext}$ is the set of boundary edges on $\partial\Omega$ and $\mathcal{A}_{int}$ is the set of interior edges in Ω. If an edge σ is not lying on $\partial\Omega$, we assume for simplicity that the edge is the unique common edge of two cells K and L, $\sigma=\partial K\bigcap\partial L$. This assumption is not necessary for the two-dimensional problems. In fact, $\partial K\bigcap\partial L$ can consist of several edges, but the method of calculating auxiliary unknowns will become a little more complicated, so we will not discuss this issue. Let $\vec{n}_{K\sigma}$ ($\vec{n}_{L\sigma}$) be the unit outer normal vector on the edge σ of cell K (L), and $\vec{n}_{K\sigma}=-\vec{n}_{L\sigma}$ for $\sigma=\partial K\bigcap\partial L$. The distance between two nodes x_A and x_B is denoted by $|AB|$. The distance between two cell-centers x_K and x_L is denoted by $|KL|$.

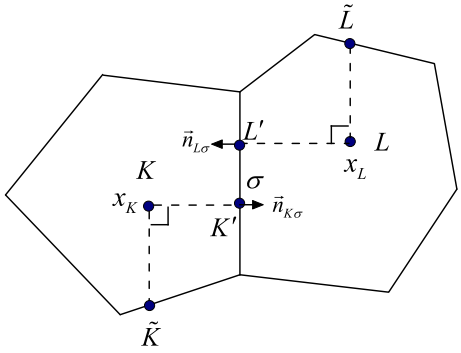

FIG. 1. *The notations of the stencil.*

Denote K'_σ and L'_σ be the orthogonal projections of x_K and x_L to the edge σ, respectively. K' and L' can be located on the extended line of σ. Draw an auxiliary line which is parallel to σ and passing $x_K(x_L)$; there will be two intersection points with $\partial K(\partial L)$. We choose one of the intersection points and denote it by $\tilde{K}_\sigma(\tilde{L}_\sigma)$ such that $\overrightarrow{x_K\tilde{K}_\sigma}$ $(\overrightarrow{x_L\tilde{L}_\sigma})$ has the same direction as $\overrightarrow{L'_\sigma K'_\sigma}(\overrightarrow{K'_\sigma L'_\sigma})$. For simplicity we omit the subscript σ when there is no confusion. See Figure 1.

We assume that

(A1) each cell K is a star-shaped polygon with respect to x_K;
(A2) there are two constants $\kappa_1 \geq \kappa_0 > 0$ such that $\kappa_1 \geq \kappa_\alpha \geq \kappa_0, \alpha \in \{e, i, r\}$;
(A3) in the domain $\Omega_0 = \Omega \backslash \Gamma$, κ_α is assumed to be smooth in Ω_0, $u_\alpha \in C^2(\Omega_0)$; at the material interface Γ, κ_α is allowed to be discontinuous, but u_α and $\kappa_\alpha \frac{\partial u_\alpha}{\partial \vec{n}}$ are continuous, $\alpha \in \{e, i, r\}$;

2.2. Construction of scheme. By using the implicit discretization and integrating (1)–(3) on cell K, according to the Green formula, we get the equations

$$\rho_K^{n+1} c_{v,K}^{\alpha,n+1}(\mathbf{u}^\alpha) \frac{u_K^{\alpha,n+1} - u_K^{\alpha,n}}{\tau} S_K + \sum_{\sigma \in \mathcal{A}_K} F_{K,\sigma}^{\alpha,n+1}(\mathbf{u}^\alpha)|\sigma| = f_K^{\alpha,n+1} S_K, \tag{7}$$

where τ is the time step, $\mathbf{u}^\alpha = (u_K^{\alpha,n+1})_{K\in\mathcal{T}}$, $\alpha \in \{e, i, r\}$, $c_{v,K}^{\alpha,n+1}(\mathbf{u}^\alpha)$ is the heat capacity of particle α for cell K at the $n+1$ time step, and

$$\begin{aligned} f_K^{e,n+1} &= (\omega_{ei})_K^{n+1}(u_K^{i,n+1} - u_K^{e,n+1}) + (\omega_{er})_K^{n+1}(u_K^{r,n+1} - u_K^{e,n+1}) \\ &\quad + (W_e)_K^{n+1}, \end{aligned} \tag{8}$$

$$f_K^{i,n+1} = (\omega_{ei})_K^{n+1}(u_K^{e,n+1} - u_K^{i,n+1}) + (W_i)_K^{n+1}, \tag{9}$$

$$f_K^{r,n+1} = (\omega_{er})_K^{n+1}(u_K^{r,n+1} - u_K^{e,n+1}). \tag{10}$$

It remains to give a discretization of the normal flux $F_{K,\sigma}^{\alpha,n+1}$, which is abbreviated to $F_{K,\sigma}^{\alpha}$ for simplicity. The discretization of $F_{K,\sigma}^{\alpha}$ is similar to [13], so we just present the main steps and omit some details.

When $\sigma \in \mathcal{A}_{ext}$, let

$$F_{K,\sigma}^{\alpha}(\mathbf{u}^\alpha) = -\kappa_K^\alpha \frac{u_{K'}^\alpha - u_K^\alpha}{|KK'|}, \tag{11}$$

where $u_{K'}^\alpha = u_\alpha(K')$ is the particle temperature u_α at $K' \in \partial\Omega$ and $\kappa_K^\alpha = \kappa_\alpha(x_K) \approx \frac{1}{S_K}\int_K \kappa_\alpha(x)dx$.

When $\sigma \in \mathcal{A}_{int}, \sigma = K|L$, we construct the flux $F^{\alpha}_{K,\sigma}$ by the following four steps.

Step 1. Construct the linear fluxes.

Let $\tilde{F}^{\alpha}_{K,\sigma} = -\kappa^{\alpha}_K \frac{u^{\alpha}_{K'} - u^{\alpha}_K}{|KK'|}$ and $\tilde{F}^{\alpha}_{L,\sigma} = \kappa^{\alpha}_L \frac{u^{\alpha}_{L'} - u^{\alpha}_L}{|LL'|}$, where $u^{\alpha}_{K'} = u_{\alpha}(K')$, $u^{\alpha}_{L'} = u_{\alpha}(L')$, $K' \in \sigma, L' \in \sigma$. We approximate the normal flux $\bar{F}^{\alpha}_{K,\sigma}$ by using a linear combination of $\tilde{F}^{\alpha}_{K,\sigma}$ and $\tilde{F}^{\alpha}_{L,\sigma}$ such that the coefficients of u^{α}_K and $-u^{\alpha}_L$ in the final expression are equal to each other. Then we get the expression $\bar{F}^{\alpha}_{K,\sigma} = \frac{\kappa^{\alpha}_{\sigma}}{|\sigma|}(u^{\alpha}_K - u^{\alpha}_L + u^{\alpha}_{L'} - u^{\alpha}_{K'}) = -\bar{F}^{\alpha}_{L,\sigma}$, where $\kappa^{\alpha}_{\sigma} = \frac{\kappa^{\alpha}_K \kappa^{\alpha}_L |\sigma|}{|KK'|\kappa^{\alpha}_L + |LL'|\kappa^{\alpha}_K}$.

Step 2. Approximate the difference term $u^{\alpha}_{L'} - u^{\alpha}_{K'}$.

We approximate the difference term $u^{\alpha}_{L'} - u^{\alpha}_{K'}$ at cells K and L, respectively. Note that the definition of $\tilde{K}$ and $\tilde{L}$. For cell K, we take the following approximation:

$$u^{\alpha}_{L'} - u^{\alpha}_{K'} \approx \frac{|K'L'|}{|K\tilde{K}|}(u^{\alpha}_K - u^{\alpha}_{\tilde{K}}). \tag{12}$$

Similarly, for cell L, we take

$$u^{\alpha}_{K'} - u^{\alpha}_{L'} \approx \frac{|K'L'|}{|L\tilde{L}|}(u^{\alpha}_L - u^{\alpha}_{\tilde{L}}). \tag{13}$$

Step 3. Calculate the unknowns at the auxiliary points $\tilde{K}$ and $\tilde{L}$.

Let $\mathcal{N}(K)$ be the following set:

$$\mathcal{N}_K = \{M | K \cap M \neq \emptyset, M \in \mathcal{T}\}, \tag{14}$$

where $K \cap M \neq \emptyset$ means that the two cells have a common vertex at least.

We calculate the unknowns at $\tilde{K}$ and $\tilde{L}$ by the convex combination of cell-centered unknowns from the set $\mathcal{N}_K$ and $\mathcal{N}_L$, respectively,

$$u^{\alpha}_{\tilde{K}} \approx \sum_{M \in \mathcal{N}_K} \gamma^{\alpha}_M u^{\alpha}_M, \tag{15}$$

$$u^{\alpha}_{\tilde{L}} \approx \sum_{N \in \mathcal{N}_L} \beta^{\alpha}_N u^{\alpha}_N, \tag{16}$$

where these weight coefficients satisfy $\gamma^{\alpha}_M > 0, \sum_M \gamma^{\alpha}_M = 1, \beta^{\alpha}_N > 0, \sum_N \beta^{\alpha}_N = 1, \alpha \in \{e, i, r\}$. The calculations of these coefficients are similar to those in [13].

Denote

$$\triangle^{\alpha}_{K,\sigma}(\mathbf{u}) = \frac{|K'L'|}{|K\tilde{K}|} \sum_{M \in \mathcal{N}_K} \gamma^{\alpha}_M (u^{\alpha}_K - u^{\alpha}_M), \tag{17}$$

$$\triangle^{\alpha}_{L,\sigma}(\mathbf{u}) = \frac{|K'L'|}{|K\tilde{K}|} \sum_{N \in \mathcal{N}_L} \beta^{\alpha}_N (u^{\alpha}_L - u^{\alpha}_N). \tag{18}$$

Then, we obtain two new single-sided normal fluxes as follows:

$$\hat{F}^{\alpha}_{K,\sigma} = \frac{\kappa^{\alpha}_{\sigma}}{|\sigma|}(u^{\alpha}_K - u^{\alpha}_L + \triangle^{\alpha}_{K,\sigma}(\mathbf{u}^{\alpha})), \tag{19}$$

$$\hat{F}^{\alpha}_{L,\sigma} = \frac{\kappa^{\alpha}_{\sigma}}{|\sigma|}(u^{\alpha}_L - u^{\alpha}_K + \triangle^{\alpha}_{L,\sigma}(\mathbf{u}^{\alpha})). \tag{20}$$

Step 4. Construct unique flux on an edge.

We obtain the final expression of the normal flux $F_{K,\sigma}^{\alpha,n+1}$ by a nonlinear combination of $\hat{F}_{K,\sigma}^{\alpha}$ and $\hat{F}_{L,\sigma}^{\alpha}$. Here the superscript $n+1$ is added to be coincident with (7).

$$\mathbf{F}_{K,\sigma}^{\alpha,n+1}(\mathbf{u}^{\alpha}) = \frac{\kappa_{\sigma}^{\alpha,n+1}}{|\sigma|}(u_K^{\alpha,n+1} - u_L^{\alpha,n+1}) + G_{K,\sigma}^{\alpha,n+1}(\mathbf{u}^{\alpha}), \tag{21}$$

where

$$G_{K,\sigma}^{\alpha,n+1}(\mathbf{u}^{\alpha}) = \begin{cases} \frac{\kappa_{\sigma}^{\alpha,n+1}}{|\sigma|} \cdot \frac{2\triangle_{L,\sigma}^{\alpha,n+1}(\mathbf{u}^{\alpha})\triangle_{K,\sigma}^{\alpha,n+1}(\mathbf{u}^{\alpha})}{\triangle_{L,\sigma}^{\alpha,n+1}(\mathbf{u}^{\alpha}) - \triangle_{K,\sigma}^{\alpha,n+1}(\mathbf{u}^{\alpha})} & \text{if } \triangle_{L,\sigma}^{\alpha,n+1}\triangle_{K,\sigma}^{\alpha,n+1} < 0, \\ 0 & \text{if } \triangle_{L,\sigma}^{\alpha,n+1}\triangle_{K,\sigma}^{\alpha,n+1} \geq 0. \end{cases} \tag{22}$$

To avoid the discontinuity of the coefficient matrix with the temperature in the nonlinear iteration, we actually use the following regularized scheme.

When $\triangle_{L,\sigma}^{\alpha,n+1}\triangle_{K,\sigma}^{\alpha,n+1} < 0$,

$$G_{K,\sigma}^{\alpha,n+1}(\mathbf{u}^{\alpha}) = \frac{\kappa_{\sigma}^{\alpha,n+1}}{|\sigma|} \cdot \frac{2|\triangle_{L,\sigma}^{\alpha,n+1}(\mathbf{u}^{\alpha})||\triangle_{K,\sigma}^{\alpha,n+1}(\mathbf{u}^{\alpha})|}{|\triangle_{L,\sigma}^{\alpha,n+1}(\mathbf{u}^{\alpha})| + |\triangle_{K,\sigma}^{\alpha,n+1}(\mathbf{u}^{\alpha})| + \varepsilon/|\triangle_{K,\sigma}^{\alpha,n+1}(\mathbf{u}^{\alpha})\triangle_{L,\sigma}^{\alpha,n+1}(\mathbf{u}^{\alpha})|}. \tag{23}$$

When $\triangle_{L,\sigma}^{\alpha,n+1}\triangle_{K,\sigma}^{\alpha,n+1} \geq 0$, $G_{K,\sigma}^{\alpha,n+1}(\mathbf{u}^{\alpha}) = 0$.

3. Calculation of auxiliary unknowns.

3.1. The perpendicular feet of the boundary edges. From the expression (11) for the boundary edge $\sigma = P_1P_2$, we can see that $u_{K'}^{\alpha}$ is an auxiliary unknown, and it should be eliminated. We use different methods to do it when K' locates in different positions. There are three cases according to different meshes.

Case 1. K' locates on the boundary of Ω; see Figure 2 (left).

When the Dirichlet boundary condition is used, $u_{K'}$ can be obtained exactly from given data. When the Neumann boundary condition is concerned, we calculate $u_{K'}$ by the unknowns at nodes P_1 and P_2, i.e., $u_{K'}^{\alpha} = \omega_1 u_{P_1}^{\alpha} + \omega_2 u_{P_2}^{\alpha}$, where $\omega_1 = \frac{|K'P_2|}{|P_1P_2|} \geq 0$, $\omega_2 = \frac{|K'P_1|}{|P_1P_2|} \geq 0$. The values $u_{P_1}^{\alpha}, u_{P_2}^{\alpha}$ are also unknown under the Neumann boundary condition. We will introduce the interpolation calculation for them in the following subsection.

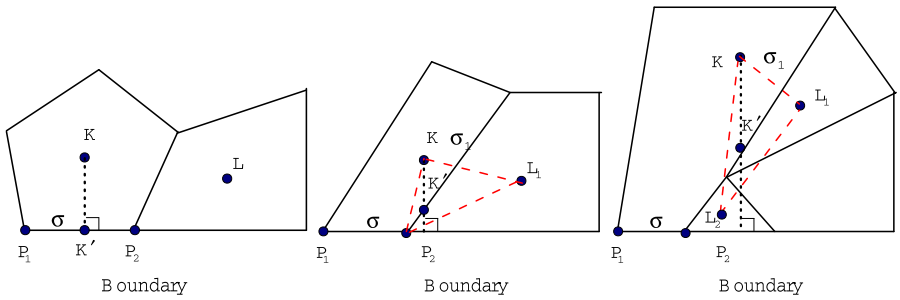

FIG. 2. *The stencil of the boundary edges.*

Case 2. K' locates on some edge σ_1 which is not a boundary edge. Assume that for the two nodes of edge σ_1, one locates on the boundary and the other does not; see Figure 2 (middle).

We choose three points P_2 and the cell-centers x_K and x_{L_1} to generate a triangle $\triangle KP_2L_1$, where $\sigma_1 = K|L_1$.

When the meshes are not distorted severely, the point K' always locates in the interior of $\triangle KP_2L_1$. We calculate $u_{K'}$ by the values at the nodes of triangle $\triangle KP_2L_1$ with the area weights, i.e., $u^\alpha_{K'} = \omega_1 u^\alpha_K + \omega_2 u^\alpha_{P_2} + \omega_3 u^\alpha_{L_1}$, $\omega_1 = \frac{S_{\triangle K'P_2L_1}}{S_{\triangle KP_2L_1}}, \omega_2 = \frac{S_{\triangle K'L_1K}}{S_{\triangle KP_2L_1}}, \omega_3 = \frac{S_{\triangle K'KP_2}}{S_{\triangle KP_2L_1}}$.

When the point K' is outside the $\triangle KP_2L_1$, we can always find one cell L_2 from the neighboring cells of L_1 such that K' locates in the interior of $\triangle KP_2L_2$. Similarly we interpolate $u_{K'}$ by u_K, u_{P_2}, u_{L_2} with area weights.

Case 3. K' locates on some edge $\sigma_1 \in \mathcal{E}_{int}$ and both nodes of edge σ_1 do not locate on the boundary; see Figure 2 (right).

In this case, we find another two cell-centers x_{L_2} and x_{L_1} such that K' locates in $\triangle KL_2L_1$, then use the inner interpolation to calculate $u_{K'}$ similarly to Case 2.

3.2. The boundary nodes. When the auxiliary points such as $\tilde{K}, K'$ are near the boundary, the unknowns on the boundary nodes $\{u_P, P \in \mathcal{E}_{ext}\}$ are always used in the interpolation formulations. To obtain a cell-centered scheme, the unknowns $\{u_P, P \in \mathcal{E}_{ext}\}$ should be eliminated.

If the Dirichlet boundary condition is considered, $\{u_P, P \in \mathcal{E}_{ext}\}$ can be obtained directly.

Our attention will be paid mainly to the case of the Neumann boundary condition.

Assume the point P locates on the boundary, and PP_1 and PP_2 are two boundary edges sharing P; see Figure 3. For the cell K, we draw an auxiliary line KK_1 perpendicular to the edge PP_1, the intersection point is $\bar{K}$, and there is $|K\bar{K}| = |\bar{K}K_1|$. For the cell L, we draw another line LL_1 such that $LL_1 \perp PP_2$ and $|L\bar{L}| = |\bar{L}L_1|$. We get lines KL, K_1L_1, KL_1, and K_1L by connecting these nodes; see Figure 3 (left).

According to the Neumann boundary condition $\kappa_\alpha \nabla u_\alpha(\mathbf{x}) \cdot \vec{n}|_{\partial\Omega} = g_\alpha(\mathbf{x}, t)$, we discretize this equation on the boundary edge PP_1 as follows:

$$-\kappa_\alpha(u^\alpha_K)\frac{u^\alpha_K - u^\alpha_{K_1}}{|KK_1|} = g_\alpha(\mathbf{x}_{\bar{K}}, t). \tag{24}$$

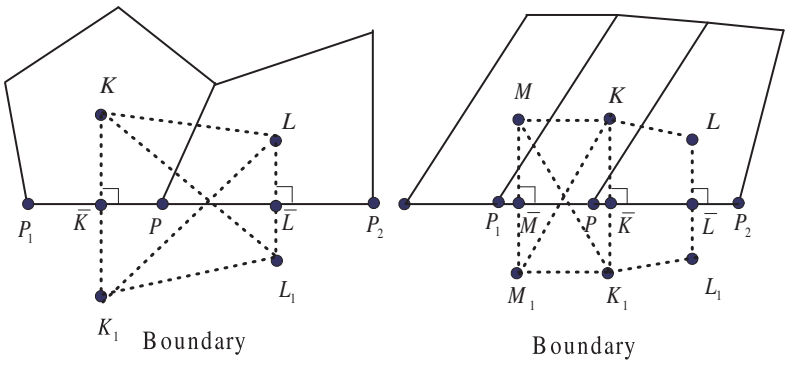

FIG. 3. *Two different interpolation stencils of the boundary nodes.*

Then, we get

$$u_{K_1}^{\alpha} = \frac{g_{\alpha}(\mathbf{x}_{\bar{K}}, t)|KK_1|}{\kappa_{\alpha}} + u_K^{\alpha}. \tag{25}$$

$u_{L_1}^{\alpha}$ is calculated similarly.

If the point P locates in the quadrangle KK_1L_1L, assume P locates in $\triangle KK_1L$ and $\triangle KK_1L_1$. We approximate two temperatures $u_{P_{\triangle KK_1L}}^{\alpha}$ and $u_{P_{\triangle KK_1L_1}}^{\alpha}$ by the values at the vertices of the triangles with area weights,

$$u_{P_{\triangle KK_1L}}^{\alpha} \approx \xi_1 u_K^{\alpha} + \xi_2 u_{K_1}^{\alpha} + \xi_3 u_L^{\alpha}, \tag{26}$$

$$u_{P_{\triangle KK_1L_1}}^{\alpha} \approx \eta_1 u_K^{\alpha} + \eta_2 u_{K_1}^{\alpha} + \eta_3 u_{L_1}^{\alpha}, \tag{27}$$

where $\{\xi_i, i = 1, 2, 3\}$ and $\{\eta_j, j = 1, 2, 3\}$ are area weights.

Then, we set

$$u_P^{\alpha} = \frac{1}{2}\left(u_{P_{\triangle KK_1L}}^{\alpha} + u_{P_{\triangle KK_1L_1}}^{\alpha}\right). \tag{28}$$

If the meshes are distorted severely, the point P may be outside the quadrangle KK_1L_1L; see Figure 3 (right). We cannot use the same interpolation method as above because some weight coefficients may be negative.

A simple way is taking inverse distance weights, i.e.,

$$u_P^{\alpha} = (\omega_1 u_K^{\alpha} + \omega_2 u_{K_1}^{\alpha} + \omega_3 u_{L_1}^{\alpha} + \omega_4 u_L^{\alpha})/T_w, \tag{29}$$

where $\omega_1 = \frac{\kappa_K^{\alpha}}{|KP|}, \omega_2 = \frac{\kappa_{K_1}^{\alpha}}{|K_1P|}, \omega_3 = \frac{\kappa_{L_1}^{\alpha}}{|L_1P|}, \omega_4 = \frac{\kappa_L^{\alpha}}{|LP|}$ and $T_w = \omega_1 + \omega_2 + \omega_3 + \omega_4$.

Another way is to find another cell M from the neighboring cells of K, such that P locates in the quadrangle KMM_1K_1; see Figure 3 (right). Then we calculate u_P^{α} by the temperatures on the vertices K, M, M_1, K_1 similarly. In the numerical tests we use the first method.

4. Theoretical results. According to (7)–(10), (21)–(22) and the calculation for the auxiliary unknowns, we obtain a nonlinear finite volume scheme of 3T radiation diffusion equations with the Dirichlet or Neumann boundary conditions. In this section, we will prove that our scheme satisfies the DMP, and there exists at least one discrete solution for the nonlinear scheme.

We rewrite our scheme with two kinds of boundary conditions. When the Dirichlet boundary condition $u_{\alpha}(\mathbf{x}, t)|_{\partial\Omega} = g_{\alpha}(\mathbf{x}, t)$ is used, the scheme can be rewritten as

$$\begin{aligned} &E_K^{\alpha,n+1}\frac{u_K^{\alpha,n+1} - u_K^{\alpha,n}}{\tau} + \sum_{L\in\mathcal{Q}_K} D_L^{\alpha,n+1}\left(u_K^{\alpha,n+1} - u_L^{\alpha,n+1}\right) \\ &+ C_K^{\alpha,n+1}\left(u_K^{\alpha,n+1} - g_d^{\alpha,n+1}\right) + \sum_{\beta\neq\alpha}\omega_{\alpha\beta}^{n+1}\left(u_K^{\alpha,n+1} - u_K^{\beta,n+1}\right) = 0, \end{aligned} \tag{30}$$

where $E_K^{\alpha,n+1} = \rho_K^{n+1} c_{v,K}^{\alpha,n+1} S_K$, $\mathcal{Q}_K$ denotes all the cells used in the discrete stencil for cell K, and $D_{K'}^{\alpha,n+1}$ is the final coefficient of the difference term $u_K^{\alpha,n+1} - u_{K'}^{\alpha,n+1}$ after combining all the discrete normal fluxes of cell K.

The term $g_d^{\alpha,n+1}$ denotes an average value of the temperatures at some points on the boundary, and its meaning can be explained in detail by the following example. See Figure 4; $\sigma \in \partial\Omega$, the perpendicular foot K' locates on $\partial\Omega$, then the discrete

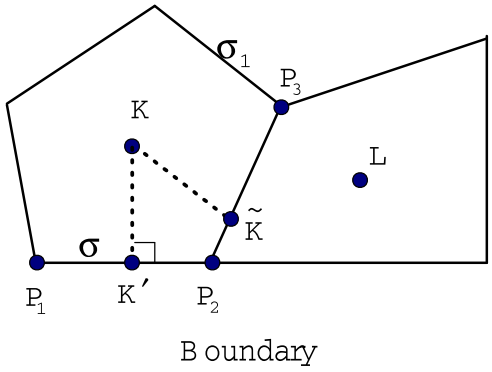

FIG. 4. *The stencil of boundary cells.*

normal flux on σ is $F_{K,\sigma}^{\alpha,n+1} = a_1(u_K^{\alpha,n+1} - u_{K'}^{\alpha,n+1})$, $a_1 \geq 0$. For the flux $F_{K,\sigma_1}^{\alpha,n+1}$ on another edge σ_1 of cell K, assume the intersection point $\tilde{K}$ locates on the edge P_2P_3, $P_2 \in \partial\Omega, P_3 \in \Omega$. Then, the difference term $a_2(u_K^{\alpha,n+1} - u_{P_2}^{\alpha,n+1})$ with $a_2 \geq 0$ will be included in $F_{K,\sigma_1}^{\alpha,n+1}$ from the construction of our scheme. Combining the two terms $F_{K,\sigma}^{\alpha,n+1}$ and $a_2(u_K^{\alpha,n+1} - u_{P_2}^{\alpha,n+1})$ of total flux of cell K, we get

$$F_{K,\sigma}^{\alpha,n+1} + a_2(u_K^{\alpha,n+1} - u_{P_2}^{\alpha,n+1}) = (a_1 + a_2)\left(u_K^{\alpha,n+1} - \left(\frac{a_1 u_{K'}^{\alpha,n+1} + a_2 u_{P_2}^{\alpha,n+1}}{a_1 + a_2}\right)\right).$$

Then,

$$g_d^{\alpha,n+1} = \frac{a_1 u_{K'}^{\alpha,n+1} + a_2 u_{P_2}^{\alpha,n+1}}{a_1 + a_2} = \frac{a_1 g_\alpha(x_{K'}, t^{n+1}) + a_2 g_\alpha(x_{P_2}, t^{n+1})}{a_1 + a_2}.$$

From the construction of our scheme (7)–(10) and (21)–(22), we can infer that all the following coefficients are nonnegative, i.e.,

$$\omega_{\alpha\beta}^{n+1} \geq 0, E_K^{\alpha,n+1} > 0, D_L^{\alpha,n+1} \geq 0, C_K^{\alpha,n+1} \geq 0 \ \ \forall \alpha, \beta \in \{e, i, r\}, L \in \mathcal{Q}_K. \tag{31}$$

Similarly we can discuss the case with Neumann boundary condition $\kappa_\alpha \nabla u_\alpha(\mathbf{x}, t) \cdot \vec{n}|_{\partial\Omega} = g_\alpha(\mathbf{x}, t)$, and rewrite our scheme as follows:

$$\begin{aligned} &E_K^{\alpha,n+1}\frac{u_K^{\alpha,n+1} - u_K^{\alpha,n}}{\tau} + \sum_{L\in\mathcal{Q}_K} D_L^{\alpha,n+1}(u_K^{\alpha,n+1} - u_L^{\alpha,n+1}) \\ &-C_K^{\alpha,n+1} g_n^{\alpha,n+1} + \sum_{\beta\neq\alpha} \omega_{\alpha\beta}^{n+1}(u_K^{\alpha,n+1} - u_K^{\beta,n+1}) = 0, \end{aligned} \tag{32}$$

where $g_n^{\alpha,n+1}$ is an inner interpolation of some values from $\{g_\alpha(\mathbf{x}_\sigma, t), \sigma \in \partial\Omega\}$. All the coefficients of (32) are nonnegative.

4.1. Discrete maximum principle. We have the following DMP property for our scheme.

THEOREM 4.1 (DMP). *Assume that the conditions* (A1)–(A3) *hold and there is no heat source for* (1)–(3)*, i.e.,* $W_e = W_i = 0$*. Let* $m = \min_{\mathbf{x}\in\bar{\Omega}}\{\varphi_e(\mathbf{x}), \varphi_i(\mathbf{x}), \varphi_r(\mathbf{x})\}$, $M = \max_{\mathbf{x}\in\bar{\Omega}}\{\varphi_e(\mathbf{x}), \varphi_i(\mathbf{x}), \varphi_r(\mathbf{x})\}$*. In the case of the Dirichlet boundary condition,*

assume $g_\alpha(\mathbf{x},t) \le M (g_\alpha(\mathbf{x},t) \ge m)\ \forall \mathbf{x} \in \partial\Omega, 0 < t \le T$*; in the case of the Neumann boundary condition, assume* $\kappa_\alpha \frac{\partial u_\alpha}{\partial \vec{n}} \le 0 (\kappa_\alpha \frac{\partial u_\alpha}{\partial \vec{n}} \ge 0)$*. Then, for both of the schemes* (30) *and* (32)*, we have*

(i) $\forall K \in \mathcal{T}, n \le N, u_K^{\alpha,n} \le M (u_K^{\alpha,n} \ge m)$*;*

(ii) *if some particle temperature of cell* K *obtains the maximum (minimum) value at time step* n_0*,* $0 < n_0 < N$*, for example, the electron temperature* $u_K^{e,n_0} = M$ $(u_K^{e,n_0} = m)$*, then*

$$u_L^{\alpha,n_1} = M (u_L^{\alpha,n_1} = m) \forall L \in \Omega \forall 0 \le n_1 \le n_0, \forall \alpha \in \{e,i,r\}. \tag{33}$$

Proof. We only give the proof of the DMP, and the discrete minimum principle can be obtained similarly. Let $v_K^{\alpha,n} = u_K^{n,\alpha} - M, \alpha \in \{e,i,r\}, 0 \le n \le N, K \in \mathcal{T}$. ∎

First we prove the result (i) with different boundary conditions.

Dirichlet boundary condition. According to (30), $\{v_K^{\alpha,n}, K \in \mathcal{T}\}$ satisfy the following equation:

$$\begin{aligned} & E_K^{\alpha,n+1} \frac{v_K^{\alpha,n+1} - v_K^{\alpha,n}}{\tau} + \sum_{K_1 \in \mathcal{Q}_K} D_{K_1}^{\alpha,n+1} (v_K^{\alpha,n+1} - v_{K'}^{\alpha,n+1}) \\ & + C_K^{\alpha,n+1} (v_K^{\alpha,n+1} - l_b^{\alpha,n+1}) + \sum_{\beta \ne \alpha} \omega_{\alpha\beta}^{n+1} (v_K^{\alpha,n+1} - v_K^{\beta,n+1}) = 0, \end{aligned} \tag{34}$$

where $l_b^{\alpha,n+1} = g_d^{\alpha,n+1} - M$. The result (i) means that $\forall K \in \mathcal{T}, n \le N$, there is $v_K^{\alpha,n} \le 0$.

We give the proof by the contradiction. Assume some particle temperature of the cell $K_0 \in \mathcal{T}$ obtains the maximum value M_0 in the whole domain at the n_0-th time step, such as the electron temperature $u_{K_0}^{e,n_0}$, $0 < n_0 < N, M_0 > M$, then $v_{K_0}^{e,n_0} = M_0 - M > 0$. Let $M_1 = M_0 - M$, then $M_1 > 0$.

According to the boundary condition, we have $g_d^{\alpha,n+1} \le M$, $l_b^{\alpha,n+1} \le 0$.

We consider the electron equation of (34) with $\alpha = e$. Because $v_{K_0}^{e,n_0}$ obtains the maximum value M_1, the following equations hold $\forall K_1 \in \mathcal{Q}_K$:

$$\begin{aligned} v_{K_0}^{e,n_0} - v_{K_0}^{e,n_0-1} \ge 0, \\ v_{K_0}^{e,n_0} - v_{K_1}^{e,n_0-1} \ge 0, \\ v_{K_0}^{e,n_0} - v_{K_1}^{i,n_0-1} \ge 0, \\ v_{K_0}^{e,n_0} - v_{K_1}^{r,n_0-1} \ge 0, \\ v_{K_0}^{e,n_0} - l_b^{\alpha,n_0} \ge 0. \end{aligned}$$

According to (31), the left part of electron equation (34) is no less than 0. So, the following propositions hold:

(1) $v_{K_0}^{e,n+1} = v_{K_0}^{e,n}$;

(2) $\forall K_1 \in \mathcal{Q}_K$, if $D_{K'}^{\alpha,n_0} > 0$, then $v_{K_0}^{e,n_0} = v_{K_1}^{e,n_0}$;

(3) if $\omega_{ei}^{n_0} > 0$, then $v_{K_0}^{e,n_0} = v_{K_0}^{i,n_0}$;

(4) if $\omega_{er}^{n_0} > 0$, then $v_{K_0}^{e,n_0} = v_{K_0}^{r,n_0}$;

(5) if $C_{K_0}^{e,n_0} > 0$, then $v_{K_0}^{e,n_0} = l_b^{e,n_0}$.

According to (21), the coefficient $D_{K_1}^{\alpha,n_0} > 0$ for the cell K_1 which shares the common edge with cell K_0. So, $v_{K_1}^{e,n_0} = v_{K_0}^{e,n_0} = M_1 > 0$, i.e., the electron temperature

of cell K_1 gets the maximum value M_0. By the same analysis for the cell K_1, the temperature of cells which have common edge with cell K_1 will get the maximum value M_0. From the connectedness of domain we can get that $v_K^{e,n_0} = M_1 > 0 \forall K \in \mathcal{T}$.

For the electron equation of (31), there must exist a cell K_2 near the boundary such that $C_{K_2}^{e,n_0} > 0$. For $v_{K_2}^{e,n_0} = M_1 > 0$ and $l_b^{e,n_0} \le 0$, we have

$$C_{K_2}^{e,n_0}(v_{K_2}^{e,n_0} - l_b^{e,n_0}) > 0.$$

For all the cells $K_3 \in P_{K_2}$, there hold

$$\begin{aligned} v_{K_2}^{e,n_0} - v_{K_2}^{e,n_0-1} &\ge 0, \\ v_{K_2}^{e,n_0} - v_{K_3}^{e,n_0-1} &\ge 0, \\ v_{K_2}^{e,n_0} - v_{K_3}^{i,n_0-1} &\ge 0, \\ v_{K_2}^{e,n_0} - v_{K_3}^{r,n_0-1} &\ge 0. \end{aligned}$$

So the left part of (34) is bigger than 0, and (34) does not hold. It is a contradiction.

Neumann boundary condition. If the Neumann boundary condition is used, then $\{v_K^{\alpha,n+1}, K \in \mathcal{T}\}$ satisfy the following equation:

$$\begin{aligned} &E_K^{\alpha,n+1} \frac{v_K^{\alpha,n+1} - v_K^{\alpha,n}}{\tau} + \sum_{K_1 \in \mathcal{Q}_K} D_{K_1}^{\alpha,n+1} \left(v_K^{\alpha,n+1} - v_{K'}^{\alpha,n+1} \right) \\ &- C_K^{\alpha,n+1} g_n^{\alpha,n+1} + \sum_{\beta \ne \alpha} \omega_{\alpha\beta}^{n+1} \left(v_K^{\alpha,n+1} - v_K^{\beta,n+1} \right) = 0. \end{aligned} \tag{35}$$

Because $g_\alpha(\mathbf{x}_\sigma, t) = \kappa_\alpha \frac{\partial u_\alpha}{\partial \vec{n}}|_\sigma \le 0$, and $g_n^{\alpha,n+1}$ is the inner interpolation of $g_\alpha(\mathbf{x}_\sigma, t)$ of some boundary edges $\sigma \in \partial\Omega$, we have $g_n^{\alpha,n+1} \le 0$. According to (31), there holds

$$-C_K^{\alpha,n+1} g_n^{\alpha,n+1} \ge 0.$$

Assume some particle temperature $u_{K_0}^{e,n_0}$ obtains the maximum value $M_0 > M$, i.e., $v_{K_0}^{e,n_0} > 0$. It will induce a contradiction by a similar proof as for the case of the Dirichlet boundary condition. Thus, the result (i) holds.

Second, we prove the result (ii). If some partial temperature such as $u_{K_0}^{e,n_0}$ gets the maximum value M, $n_0 < N$. Repeating the proof of (i), we can infer that the electron temperatures of all the cells at the $n_0 - 1$ time step also get the maximum value.

Besides, because $\omega_{ei}^{n_0} > 0, \omega_{er}^{n_0} > 0$, and

$$\omega_{ei}^{n_0}(u_{K_0}^{e,n_0} - u_{K_0}^{i,n_0}) = 0, \tag{36}$$

$$\omega_{ei}^{n_0}(u_{K_0}^{e,n_0} - u_{K_0}^{r,n_0}) = 0, \tag{37}$$

there are $u_{K_0}^{i,n_0} = M$ and $u_{K_0}^{r,n_0} = M$. By the similar analysis for the discrete schemes of ion and photo equations on the cell K_0, we have

$$u_K^{\alpha,n_1} = M \, \forall K \in \mathcal{T}, n_1 \le n_0, \alpha \in \{e, i, r\}. \tag{38}$$

The result (ii) holds.

4.2. Existence of solution. In this subsection, we only prove the existence of a solution for our scheme with the Dirichlet boundary condition. The proof of that with the Neumann boundary condition is similar.

THEOREM 4.2 (existence). *Assume that the conditions* (A1)–(A3) *hold and there is no heat source for* (1)–(3), *i.e.,* $W_e = W_i = 0$. *Let* $m = \min_{\mathbf{x}\in\bar{\Omega}}\{\varphi_e(\mathbf{x}), \varphi_i(\mathbf{x}), \varphi_r(\mathbf{x})\}$, $M = \max_{\mathbf{x}\in\bar{\Omega}}\{\varphi_e(\mathbf{x}), \varphi_i(\mathbf{x}), \varphi_r(\mathbf{x})\}$. Assume the Dirichlet boundary condition satisfies $m \le g_\alpha(\mathbf{x}, t) \le M$, $\mathbf{x} \in \Omega, 0 < t \le T$. We have

(i) there exists at least a discrete solution $u_K^\alpha, K \in \mathcal{T}, \alpha \in \{e, i, r\}$ for the nonlinear scheme (7)–(10), (21)–(22);
(ii) $\forall K \in \mathcal{T}, \forall \alpha \in \{e, i, r\}, m \le u_K^\alpha \le M$.

Proof. Define a closed convex set $\mathcal{E} \in R^{3N}$ as follows:

$$\mathcal{E} = \{\bar{\mathbf{w}} = (w_K^e, w_K^i, w_K^r, \cdots) \in R^{3N} : m \le w_K^\alpha \le M, K \in \mathcal{T}, \alpha \in \{e, i, r\}\}, \tag{39}$$

where N is the number of cells in $\mathcal{T}$.

Define a map $T : \mathcal{E} \to R^{3N}$ $\forall \bar{\mathbf{w}} \in \mathcal{E}$, $\bar{\mathbf{u}} = T\bar{\mathbf{w}}$ is the solution of the following linear system:

$$\begin{aligned} &\rho_K^{n+1} c_{v,K}^{\alpha,n+1}(\bar{\mathbf{w}}) \frac{\bar{\mathbf{u}}_K^{\alpha,n+1} - \bar{\mathbf{u}}_K^{\alpha,n}}{\tau} S_K + \sum_{\sigma\in\mathcal{A}_K} F_{K,\sigma}^{\alpha,n+1}(\bar{\mathbf{u}}, \bar{\mathbf{w}})|\sigma| \\ &= f_K^{\alpha,n+1}(\bar{\mathbf{u}}, \bar{\mathbf{w}}) S_K, \qquad \alpha \in \{e, i, r\}, K \in \mathcal{T}, \end{aligned} \tag{40}$$

where

$$f_K^{e,n+1}(\bar{\mathbf{u}}, \bar{\mathbf{w}}) = \omega_{ei}(\bar{\mathbf{w}})_K^{n+1}(\bar{u}_K^{i,n+1} - \bar{u}_K^{e,n+1}) + \omega_{er}(\bar{\mathbf{w}})_K^{n+1}(\bar{u}_K^{r,n+1} - \bar{u}_K^{e,n+1}), \tag{41}$$

$$f_K^{i,n+1}(\bar{\mathbf{u}}, \bar{\mathbf{w}}) = \omega_{ei}(\bar{\mathbf{w}})_K^{n+1}(\bar{u}_K^{e,n+1} - \bar{u}_K^{i,n+1}), \tag{42}$$

$$f_K^{r,n+1}(\bar{\mathbf{u}}, \bar{\mathbf{w}}) = \omega_{er}(\bar{\mathbf{w}})_K^{n+1}(\bar{u}_K^{r,n+1} - \bar{u}_K^{e,n+1}). \tag{43}$$

For $\sigma = K|L \in \mathcal{A}_{int}$,

$$F_{K,\sigma}^{\alpha,n+1}(\bar{\mathbf{u}}, \bar{\mathbf{w}}) = \frac{\kappa(w_\sigma^{\alpha,n+1})}{|\sigma|}(\bar{u}_K^{\alpha,n+1} - \bar{u}_L^{\alpha,n+1}) + G_{K,\sigma}^{\alpha,n+1}(\bar{\mathbf{u}}, \bar{\mathbf{w}}) \tag{44}$$

and

$$G_{K,\sigma}^{\alpha,n+1}(\bar{\mathbf{u}}, \bar{\mathbf{w}}) = \begin{cases} \frac{2\triangle_{L,\sigma}^{n+1}(\bar{\mathbf{w}})\triangle_{K,\sigma}^{\alpha,n+1}(\bar{\mathbf{u}})}{\triangle_{L,\sigma}^{\alpha,n+1}(\bar{\mathbf{w}}) - \triangle_{K,\sigma}^{\alpha,n+1}(\bar{\mathbf{w}})} & \text{if } \triangle_{L,\sigma}^{\alpha,n+1}(\bar{\mathbf{w}})\triangle_{K,\sigma}^{\alpha,n+1}(\bar{\mathbf{w}}) < 0, \\ 0 & \text{if } \triangle_{L,\sigma}^{\alpha,n+1}(\bar{\mathbf{w}})\triangle_{K,\sigma}^{\alpha,n+1}(\bar{\mathbf{w}}) \ge 0. \end{cases} \tag{45}$$

For $\sigma \in \mathcal{A}_{ext}$,

$$F_{K,\sigma}^{\alpha,n+1}(\bar{\mathbf{u}}, \bar{\mathbf{w}}) = \kappa(u_K^{\alpha,n+1}) \frac{(\bar{u}_K^{\alpha,n+1} - \bar{u}_{K'}^{\alpha,n+1})}{|KK'|}. \tag{46}$$

The linear system (40) is abbreviated to $A_{\bar{\mathbf{w}}}\bar{\mathbf{u}} = l$, where $A_{\bar{\mathbf{w}}} \in R^{3N\times 3N}$, $\bar{\mathbf{u}} \in R^{3N}$, $l \in R^{3N}$. From the expression of the discrete normal fluxes (44), we can see that the matrix $A_{\bar{\mathbf{w}}}$ is irreducible and diagonally dominant. According to the Taussky theorem (see [19]), $A_{\bar{\mathbf{w}}}$ is invertible. So, for each $\mathbf{w} \in$ E, there is only one solution $\bar{\mathbf{u}}$ for (40) and the map T is well defined. Similar to the proof of Theorem 1 for the nonlinear scheme (30), we can obtain the DMP property for the linear scheme (40). So, there holds $\bar{\mathbf{u}} = T\bar{\mathbf{w}} \in \mathcal{E}$, for each $\bar{\mathbf{w}} \in \mathcal{E}$.

From the expression of the discrete normal fluxes $F_{K,\sigma}^{\alpha,n+1}(\bar{\mathbf{u}},\bar{\mathbf{w}})$, we can see that the map T may be not continuous due to the discontinuity of $\frac{2\triangle_{L,\sigma}(\bar{\mathbf{w}})}{\triangle_{L,\sigma}(\bar{\mathbf{w}})-\triangle_{K,\sigma}(\bar{\mathbf{w}})}$ with respect to $\bar{\mathbf{w}}$. So, we consider the regularized map T_ε as follows: $\forall\varepsilon>0, T_\varepsilon:\mathcal{E}\to R^{3N}$, where $\forall\bar{\mathbf{w}}\in\mathcal{E}$, $\bar{\mathbf{u}}=T_\varepsilon\bar{\mathbf{w}}$ is defined to be the solution of the linear scheme

$$\begin{aligned}&\rho_K^{n+1}c_{v,K}^{\alpha,n+1}(\bar{\mathbf{w}})\frac{\bar{\mathbf{u}}_K^{\alpha,n+1}-\bar{\mathbf{u}}_K^{\alpha,n}}{\tau}S_K+\sum_{\sigma\in\mathcal{A}_K}(F^\varepsilon)_{K,\sigma}^{\alpha,n+1}(\bar{\mathbf{u}},\bar{\mathbf{w}})|\sigma|\\&=f_K^{\alpha,n+1}(\bar{\mathbf{u}},\bar{\mathbf{w}})S_K,\qquad\alpha\in\{e,i,r\},K\in\mathcal{T},\end{aligned}\tag{47}$$

where for the inner edge $\sigma=K|L\in\mathcal{A}_{int}$,

$$(F^\varepsilon)_{K,\sigma}^{\alpha,n+1}(\bar{\mathbf{u}},\bar{\mathbf{w}})=\kappa_\sigma^{\alpha,n+1}(\bar{\mathbf{w}})(\bar{u}_K^{\alpha,n+1}-\bar{u}_L^{\alpha,n+1})+(G^\varepsilon)_{K,\sigma}^{\alpha,n+1}(\bar{\mathbf{u}},\bar{\mathbf{w}}).\tag{48}$$

For the boundary edge $\sigma=K|L\in\mathcal{A}_{ext}$,

$$(F^\varepsilon)_{K,\sigma}^{\alpha,n+1}(\bar{\mathbf{u}},\bar{\mathbf{w}})=F_{K,\sigma}^{\alpha,n+1}(\bar{\mathbf{u}},\bar{\mathbf{w}}).\tag{49}$$

If $\triangle_{L,\sigma}^{\alpha,n+1}(\bar{\mathbf{w}})\triangle_{K,\sigma}^{\alpha,n+1}(\bar{\mathbf{w}})<0$, then

$$(G^\varepsilon)_{K,\sigma}^{\alpha,n+1}(\bar{\mathbf{u}},\bar{\mathbf{w}})=\frac{2|\triangle_{L,\sigma}^{\alpha,n+1}(\bar{\mathbf{w}})|\triangle_{K,\sigma}^{\alpha,n+1}(\bar{\mathbf{u}})}{|\triangle_{L,\sigma}^{\alpha,n+1}(\bar{\mathbf{w}})|+|\triangle_{K,\sigma}^{\alpha,n+1}(\bar{\mathbf{w}})|+\varepsilon/|\triangle_{K,\sigma}^{\alpha,n+1}(\bar{\mathbf{w}})\triangle_{L,\sigma}^{\alpha,n+1}(\bar{\mathbf{w}})|};\tag{50}$$

if $\triangle_{L,\sigma}^{\alpha,n+1}(\bar{\mathbf{w}})\triangle_{K,\sigma}^{\alpha,n+1}(\bar{\mathbf{w}})\geq 0$, then

$$(G^\varepsilon)_{K,\sigma}^{\alpha,n+1}(\bar{\mathbf{u}},\bar{\mathbf{w}})=0.\tag{51}$$

The linear system (47)–(49) is abbreviated to $A_{\bar{\mathbf{w}}}^\varepsilon\bar{\mathbf{u}}=l^\varepsilon$, where $A_{\bar{\mathbf{w}}}^\varepsilon\in R^{3N\times 3N}$, $\bar{\mathbf{u}}\in R^{3N}, l^\varepsilon\in R^{3N}$.

The matrix $A_{\bar{\mathbf{w}}}^\varepsilon$ is irreducible and diagonally dominant, thus it is invertible by the Taussky theorem. So, there is only one solution for (47) and the map T_ε is well defined.

Similar to the proof of Theorem 4.1, we have

$$\forall\bar{\mathbf{w}}\in\mathcal{E},\bar{\mathbf{u}}=T_\varepsilon\bar{\mathbf{w}}\in\mathcal{E}.\tag{52}$$

Because of the regularization in (50), the matrix $A_{\bar{\mathbf{w}}}^\varepsilon$ is continuous with respect to $\bar{\mathbf{w}}$, i.e., as $\bar{\mathbf{w}}_n\to\bar{\mathbf{w}}_0$, we get $A_{\bar{\mathbf{w}}_n}^\varepsilon\to A_{\bar{\mathbf{w}}_0}^\varepsilon$. Since the inverse operator of the matrix is continuous, we get $(A_{\bar{\mathbf{w}}_n}^\varepsilon)^{-1}\to(A_{\bar{\mathbf{w}}_0}^\varepsilon)^{-1}, n\to\infty$. It follows that $T_\varepsilon\bar{\mathbf{w}}_n\to T_\varepsilon\bar{\mathbf{w}}_0, n\to\infty$. So, the map T_ε is continuous.

By the Brouwer's fixed point theorem, there exists a fixed point $\bar{\mathbf{u}}_\varepsilon$ in $\mathcal{E}$, i.e., $T_\varepsilon\bar{\mathbf{u}}_\varepsilon=\bar{\mathbf{u}}_\varepsilon$. So, $\bar{\mathbf{u}}_\varepsilon$ satisfies

$$\begin{aligned}&\rho_K^{n+1}c_{v,K}^{\alpha,n+1}(\bar{\mathbf{u}}_\varepsilon)\frac{(\bar{\mathbf{u}}_\varepsilon)_K^{\alpha,n+1}-(\bar{\mathbf{u}}_\varepsilon)_K^{\alpha,n}}{\tau}S_K+\sum_{\sigma\in\mathcal{A}_K}(F^\varepsilon)_{K,\sigma}^{\alpha,n+1}(\bar{\mathbf{u}}_\varepsilon,\bar{\mathbf{u}}_\varepsilon)|\sigma|\\&=f_K^{\alpha,n+1}(\bar{\mathbf{u}}_\varepsilon,\bar{\mathbf{u}}_\varepsilon)S_K\forall K\in\mathcal{T},\alpha\in\{e,i,r\},\end{aligned}$$

and $m\leq(\bar{u}_\varepsilon)_K^{\alpha,n+1}\leq M\forall K\in\mathcal{T},\alpha\in\{e,i,r\}$. By the Weistrass theorem, there is a subsequence $\bar{\mathbf{u}}_{\varepsilon_n}$ of the sequence $\bar{\mathbf{u}}_\varepsilon$, such that $\bar{\mathbf{u}}_{\varepsilon_n}\to\tilde{\mathbf{u}}\in\mathcal{E}, n\to\infty$. For this subsequence, we have

$$\begin{aligned}&\triangle_{K,\sigma}^{\alpha,n+1}(\bar{\mathbf{u}}_{\varepsilon_n})\to\triangle_{K,\sigma}^{\alpha,n+1}(\tilde{\mathbf{u}}),\\&\triangle_{L,\sigma}^{\alpha,n+1}(\bar{\mathbf{u}}_{\varepsilon_n})\to\triangle_{L,\sigma}^{\alpha,n+1}(\tilde{\mathbf{u}}),\\&(G^{\varepsilon_n})_{K,\sigma}^{\alpha,n+1}(\bar{\mathbf{u}}_{\varepsilon_n},\bar{\mathbf{u}}_{\varepsilon_n})\to G_{K,\sigma}^{\alpha,n+1}(\tilde{\mathbf{u}},\tilde{\mathbf{u}}),\\&(G^{\varepsilon_n})_{L,\sigma}^{\alpha,n+1}(\bar{\mathbf{u}}_{\varepsilon_n},\bar{\mathbf{u}}_{\varepsilon_n})\to G_{L,\sigma}^{\alpha,n+1}(\tilde{\mathbf{u}},\tilde{\mathbf{u}}).\end{aligned}$$

This means that $\tilde{\mathbf{u}}$ is the solution of the nonlinear scheme (7)–(10) and (21)–(22). Therefore the result (i) is proved. The result (ii) is obvious from the proof of (i). ∎

Remark 4.3. In [4], the topological degree theory was used to prove the existence theorem for the finite volume scheme preserving the DMP without using regularization for the map T.

Remark 4.4. From the proof of Theorems 4.1 and 4.2, we can see that for our scheme there is no severe restriction on the size of the time step as the stability condition of the explicit scheme.

4.3. Nonlinear iteration. A nonlinear algebraic system $A(\mathbf{u})\mathbf{u} = l(\mathbf{u})$ is formed by the scheme (7)–(10) and (21)–(22), where $\mathbf{u} = (u_K^e, u_K^i, u_K^r)_{K\in\mathcal{T}}$. We solve it by the Picard iteration: choose a small number ε_{non} and initial vector $\mathbf{u}_0$ and perform the following procedure recurrently:

(1) Solve $A(\mathbf{u}^s)\mathbf{u}^{s+1} = l(\mathbf{u}^s)$, $s = 0, 1, 2, \ldots$,

(2) When $\|A(\mathbf{u}^{s+1})\mathbf{u}^{s+1} - l(\mathbf{u}^{s+1})\| \le \varepsilon_{non}$, the nonlinear iteration stops.

At each nonlinear iteration step, for the linear algebraic system $A(\mathbf{u}^s)\mathbf{u}^{s+1} = l(\mathbf{u}^s)$, the matrix $A(\mathbf{u}^s)$ and the vector $l(\mathbf{u}^s)$ are generated by the following iteration equations:

$$\rho_K c_{v,K}^{\alpha,s}\frac{u_K^{\alpha,s+1} - u_K^{\alpha,n}}{\tau}S_K + \sum_{\sigma\in\mathcal{A}_K} F_{K,\sigma}^{\alpha,s+1}(\mathbf{u}^s)|\sigma| + \sum_{\beta\neq\alpha}\omega_{\alpha\beta}(\mathbf{u}^s)u_K^{\beta,s+1} = W_K^{\alpha,s}S_K \quad \forall K\in\mathcal{T}, \alpha\in\{e,i,r\}, \tag{53}$$

where, if $G_{L,\sigma}^{\alpha,s}(\mathbf{u})G_{K,\sigma}^{\alpha,s}(\mathbf{u}) < 0$,

$$F_{K,\sigma}^{\alpha,s+1}(\mathbf{u}) = \kappa(\mathbf{u}_\sigma^{\alpha,s})(u_K^{\alpha,s+1} - u_L^{\alpha,s+1})|\sigma| + \frac{2G_{L,\sigma}^{\alpha,s}(\mathbf{u})}{G_{L,\sigma}^{\alpha,s}(\mathbf{u}) - G_{K,\sigma}^{\alpha,s}(\mathbf{u})}G_{K,\sigma}^{\alpha,s+1}(\mathbf{u}); \tag{54}$$

if $G_{L,\sigma}^{\alpha,s}(\mathbf{u})G_{K,\sigma}^{\alpha,s}(\mathbf{u}) \ge 0$, $F_{K,\sigma}^{\alpha,s+1}(\mathbf{u}) = 0$.

Here the superscript s of f^s represents the unknown value f at the sth nonlinear iteration step. The linear algebraic system is solved by the biconjugate gradient stabilized method. When the residual error of the linear system is smaller than ε_{lin}, the linear iteration stops.

From the expression (54), we can see that if $G_{L,\sigma}(\mathbf{u}^{\alpha,s})G_{K,\sigma}(\mathbf{u}^{\alpha,s}) < 0$, there is

$$F_{K,\sigma}^{\alpha,s+1}(\mathbf{u}) \neq F_{L,\sigma}^{\alpha,s+1}(\mathbf{u}), \quad \sigma = K|L.$$

The two fluxes on each side of the interior edge are not exactly the same, i.e., they differ by one iteration step from each other. However, our numerical tests will show that the conservation errors are very small after the nonlinear iteration converges at each time step.

5. Numerical experiments. Numerical experiments are presented in this section. The computational domain $\Omega = (0,1)\times(0,1)$ for the following Model 1 and Model 2, $\Omega = (0,300)\times(0,300)$ for Model 3, and $\varepsilon_{non} = 1.0\times10^{-8}$, $\varepsilon_{lin} = 1.0\times10^{-12}$, $\varepsilon = 10^{-10}$ in the scheme (23).

For the solution $\mathbf{u} = (u_K^e, u_K^i, u_K^r)_{K\in\mathcal{T}}$, the discrete L_2-norm to evaluate approximate errors is denoted by

$$\varepsilon_2^{\mathbf{u}} = \left[\sum_\alpha\sum_{K\in\mathcal{T}}(u_K^\alpha - u_\alpha(x_K))^2 S_K\right]^{1/2},$$

where u_K^α is the numerical temperature of the particle α at x_K, and $u_\alpha(x_K)$ is the exact temperature.

For the flux $\mathbf{F}$, the discrete L_2-norm is defined by

$$\varepsilon_2^{\mathbf{F}} = \left[\sum_\alpha \sum_{\sigma \in \mathcal{A}} (\mathbf{F}_{K,\sigma}^\alpha |\sigma| - \mathcal{F}_{K,\sigma}^\alpha |\sigma|)^2 \right]^{1/2},$$

where $\mathbf{F}_{K,\sigma}^\alpha$ is the numerical flux of the particle α at the edge σ, and the $\mathcal{F}_{K,\sigma}^\alpha$ is the exact flux.

The conservation error is measured for nonsteady 3T problems by

$$\varepsilon_{con}^{\mathbf{u}} = \left| \sum_{K \in \mathcal{T}} \sum_\alpha (u_K^{\alpha,N} - u_K^{\alpha,0}) S_K + \sum_{n=1}^N \sum_\alpha \sum_{\sigma \in \partial\Omega} \mathbf{F}_\sigma^{\alpha,n} \tau - \sum_{n=1}^N \sum_\alpha \sum_{K \in \mathcal{T}} f_K^{\alpha,n+1} \tau S_K \right|.$$

5.1. Accuracy and conservation. We test the accuracy of our scheme with a smooth coefficient problem.

Model 1. We consider the linear 3T problem (1)–(3), where $\rho = 1, c_{ve} = c_{vi} = c_{vr} = 1, \kappa_e = \kappa_i = \kappa_r = 1, \omega_{ei} = \omega_{er} = 1$, and the exact solutions are $u_e = e^t(x_1^2 + 1)(x_2^2 + 1), u_i = e^t(2x_1^2 + 1)(x_2^2 + 1), u_r = e^t(2x_1^2 + 1)(2x_2^2 + 1)$, $T = 1.0$. We use random quadrilateral meshes; see Figure 5 (left). The meshes partition is $k \times k, k = 8, 16, 32, 64$. Define the space size $h = \frac{1}{k}$. In order to test the space accuracy, the time step τ is chosen to guarantee that $\frac{\tau}{h^2}$ is a constant under different mesh partitions. Both the Dirichlet boundary condition and the Neumann one are considered.

In the Tables 1, 2, and 3, we present the convergence results of electron, ion, and photon temperatures when the Dirichlet boundary condition is used; $it^\sharp$ is the average

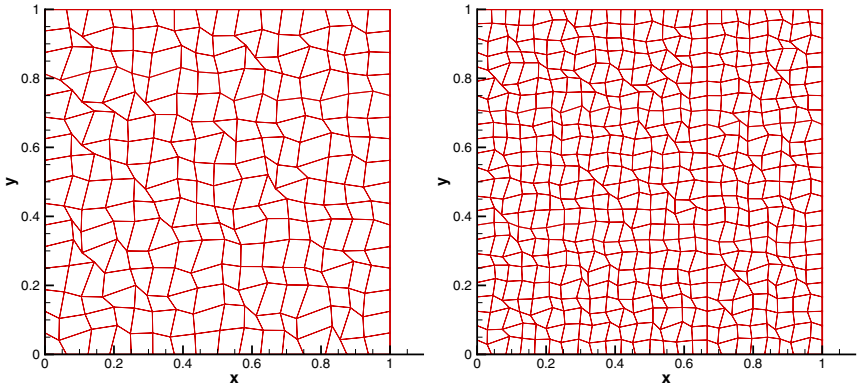

FIG. 5. *Random quadrilateral meshes (left) and discontinuous random quadrilateral meshes (right).*

TABLE 1

Convergence rates of electron temperature computed by our scheme for Model 1 *with Dirichlet boundary condition.*

Meshes	τ	$\varepsilon_2^{\mathbf{u}_e}$	Rate	$\varepsilon_2^{\mathbf{F}_e}$	Rate	$it^\sharp$
8×8	0.01	5.132e-3	-	0.285	-	11.1
16×16	2.5e-3	1.292e-3	1.99	0.138	1.04	7.7
32×32	6.25e-4	3.472e-4	1.89	6.542e-2	1.07	6.4
64×64	1.5625e-4	8.343e-5	2.05	3.212e-2	1.02	4.1

TABLE 2

Convergence rates of ion temperature computed by our scheme for Model 1 *with Dirichlet boundary condition.*

Meshes	τ	$\varepsilon_2^{\mathbf{u}_i}$	Rate	$\varepsilon_2^{\mathbf{F}_i}$	Rate
8×8	0.01	5.903e-3	-	0.479	-
16×16	2.5e-3	1.704e-3	1.79	0.228	1.07
32×32	6.25e-4	4.320e-4	1.98	0.107	1.09
64×64	1.5625e-4	1.057e-4	2.03	5.197e-2	1.04

TABLE 3

Convergence rates of photon temperature computed by our scheme for Model 1 *with Dirichlet boundary condition.*

Meshes	τ	$\varepsilon_2^{\mathbf{u}_r}$	Rate	$\varepsilon_2^{\mathbf{F}_r}$	Rate
8×8	0.01	8.026e-3	-	0.820	-
16×16	2.5e-3	2.132e-3	1.91	0.392	1.06
32×32	6.25e-4	5.564e-4	1.94	0.185	1.08
64×64	1.5625e-4	1.32e-4	2.07	9.24e-2	1.00

TABLE 4

Convergence rates of electron temperature computed by our scheme and NPS for Model 1 *with Neumann boundary condition.*

Scheme	Meshes	τ	$\varepsilon_2^{\mathbf{u}_e}$	Rate	$\varepsilon_2^{\mathbf{F}_e}$	Rate	$it^\sharp$
Our scheme	8×8	0.01	6.454e-3	-	0.999	-	13.7
	16×16	2.5e-3	1.248e-3	2.37	0.526	0.92	8.9
	32×32	6.25e-4	3.297e-4	1.92	0.274	0.94	6.9
	64×64	1.5625e-4	7.088e-5	2.21	0.151	0.86	4.1
NPS	8×8	0.01	4.812e-3	-	1.040	-	8.1
	16×16	2.5e-3	1.115e-3	2.10	0.535	0.96	4.7
	32×32	6.25e-4	2.865e-4	1.96	0.280	0.93	3.7
	64×64	1.5625e-4	7.145e-5	2.00	0.152	0.88	1.4

TABLE 5

Convergence rates of ion temperature computed by our scheme and NPS for Model 1 *with Neumann boundary condition.*

Scheme	Meshes	τ	$\varepsilon_2^{\mathbf{u}_e}$	Rate	$\varepsilon_2^{\mathbf{F}_e}$	Rate
Our scheme	8×8	0.01	6.557e-3	-	1.484	-
	16×16	2.5e-3	1.166e-3	2.49	0.817	0.86
	32×32	6.25e-4	3.344e-4	1.80	0.428	0.93
	64×64	1.5625e-4	8.690e-5	1.94	0.228	0.91
NPS	8×8	0.01	4.487e-3	-	1.556	-
	16×16	2.5e-3	1.025e-3	2.13	0.831	0.90
	32×32	6.25e-4	2.684e-4	1.93	0.435	0.93
	64×64	1.5625e-4	6.708e-5	2.00	0.230	0.92

number of Picard iterations. It shows that our scheme obtains second-order accuracy for all the particle temperatures and first-order accuracy for the fluxes.

We also test our scheme by this model with the Neumann boundary condition. In addition, we compare our scheme with the nine-point scheme (NPS; see [11]). The results are shown in Tables 4, 5, and 6. We can see that our scheme and NPS both obtain second-order accuracy for the temperatures and first-order accuracy for the fluxes when the Neumann boundary condition is used. The average number of Picard iterations of our scheme is more than that of NPS. Note that the tangential flux of NPS is computed by the values at the last Picard iteration step, so we also need nonlinear iteration for this linear model.

TABLE 6
Convergence rates of photon temperature computed by our scheme and NPS for Model 1 *with Neumann boundary condition.*

Scheme	Meshes	τ	$\varepsilon_2^{\mathbf{u}_e}$	Rate	$\varepsilon_2^{\mathbf{F}_e}$	Rate
Our scheme	8×8	0.01	7.227e-3	-	2.702	-
	16×16	2.5e-3	1.400e-3	2.36	1.402	0.95
	32×32	6.25e-4	3.784e-4	1.88	0.744	0.91
	64×64	1.5625e-4	1.046e-4	1.85	0.412	0.85
NPS	8×8	0.01	5.147e-3	-	2.796	-
	16×16	2.5e-3	1.135e-3	2.18	1.423	0.97
	32×32	6.25e-4	3.048e-4	1.90	0.755	0.91
	64×64	1.5625e-4	7.578e-5	2.00	0.415	0.86

Model 2. We test the accuracy and the conservation of our scheme by solving the following steady problem with the discontinuous diffusion coefficient:

$$\kappa_e = \begin{cases} 4, & (x,y)\in\Omega_1,\\ 1, & (x,y)\in\Omega_2. \end{cases} \quad \kappa_i = \begin{cases} 4, & (x,y)\in\Omega_1,\\ 1, & (x,y)\in\Omega_2. \end{cases} \quad \kappa_r = \begin{cases} 7, & (x,y)\in\Omega_1,\\ 1, & (x,y)\in\Omega_2. \end{cases}$$

The coefficients $\omega_{ei} = \omega_{er} = \pi^2$. For this model, the exact solutions are

$$u_e = \begin{cases} \sin(\pi x)\sin(2\pi y), & (x,y)\in\Omega_1,\\ \sin(4\pi x)\sin(2\pi y), & (x,y)\in\Omega_2. \end{cases}$$
$$u_i = \begin{cases} \sin(\pi x)(\sin(2\pi y)+1), & (x,y)\in\Omega_1,\\ \sin(4\pi x)(\sin(2\pi y)+1), & (x,y)\in\Omega_2. \end{cases}$$
$$u_r = \begin{cases} \sin(\pi x)(\sin(2\pi y)+1), & (x,y)\in\Omega_1,\\ \sin(7\pi x)(\sin(2\pi y)+1), & (x,y)\in\Omega_2, \end{cases}$$

where $\Omega_1 = (0,\frac{2}{3}]\times(0,1)$, $\Omega_2 = (\frac{2}{3},1]\times(0,1)$. The Dirichlet boundary conditions and source terms are calculated by the exact solutions. We use the random quadrilateral meshes; see Figure 5 (right).

From the numerical errors shown in Tables 7, 8 and 9, it can be seen that our scheme obtains second-order accuracy for the solutions and first-order accuracy for the fluxes for this discontinuous 3T model. This result shows that our interpolation calculation for the auxiliary points does not destroy the accuracy of the scheme.

Table 10 gives the conservation errors for this model. They are very small and approximate to the threshold value of the nonlinear iteration.

TABLE 7
Convergence rates of electron temperature for Model 2.

Meshes	$\varepsilon_2^{\mathbf{u}_e}$	Rate	$\varepsilon_2^{\mathbf{F}_e}$	Rate	$it^\sharp$
12×12	5.382e-2	-	0.956	-	17
24×24	1.302e-2	2.04	0.409	1.22	19
48×48	3.614e-3	1.85	0.182	1.16	18
96×96	7.799e-4	2.21	6.845e-2	1.41	19
192×192	2.197e-4	1.83	3.131e-2	1.12	20

TABLE 8
Convergence rates of ion temperature for Model 2.

Meshes	$\varepsilon_2^{\mathbf{u}_i}$	Rate	$\varepsilon_2^{\mathbf{F}_i}$	Rate
12×12	5.200e-2	-	1.399	-
24×24	1.464e-2	1.83	0.577	1.27
48×48	3.729e-3	1.97	0.255	1.17
96×96	9.346e-4	1.99	9.486e-2	1.42
192×192	2.522e-4	1.89	5.08e-2	0.9

TABLE 9
Convergence rates of photon temperature for Model 2.

Meshes	$\varepsilon_2^{\mathbf{u}_r}$	Rate	$\varepsilon_2^{\mathbf{F}_r}$	Rate
12×12	0.189	-	4.293	-
24×24	4.283e-2	2.14	1.761	1.28
48×48	1.057e-2	2.02	0.710	1.30
96×96	2.565e-3	2.04	0.280	1.34
192×192	6.289e-4	2.02	0.144	0.96

TABLE 10
The conservation errors of our scheme for Model 2.

Meshes	ε_{con}^{u}
12×12	-1.135e-8
24×24	2.639e-8
48×48	-5.030e-8
96×96	-5.418e-8
192×192	5.040e-8

5.2. Discrete maximum principle. We calculate the following 3T problem to test the positivity-preserving property of our scheme, which will be compared with the NPS. It is known that the NPS does not satisfy the DMP. In each nonlinear iteration step, the solutions of linear system solved by the NPS may be negative. So, we just need to use a simple 3T equation with all the coefficients being constants to compare our scheme with the NPS.

Model 3. Consider the 3T problem with two different materials A and B. The subdomain with the material A is $\Omega_1 = (0, 300) \times (0, 250)$, the subdomain with the material B is $\Omega_2 = (0, 300) \times (250, 300)$, the computational domain $\Omega = \Omega_1 \bigcup \Omega_2$. The initial conditions are $\rho_A = 0.05, \rho_B = 1.0, (\varphi_\alpha)_A = (\varphi_\alpha)_B = 3.0 \times 10^{-4}, \alpha \in \{e, i, r\}$. The diffusion coefficients are $(\kappa_e)_A = 10, (\kappa_i)_A = 10, (\kappa_r)_A = 100, (\kappa_e)_B = 10, (\kappa_i)_B = 10, (\kappa_r)_B = 10$.

The boundary condition is as follows: for the electron and ion equations, there is no flux on the boundary edges, i.e., $\frac{\partial u_\alpha}{\partial \vec{n}}|_{\partial\Omega} = 0, \alpha \in \{e, i\}$; for the photon equation, the Dirichlet condition $u_r|_{x=0} = 100$ is used on the left boundary edges, and the Neumann condition $\frac{\partial u_r}{\partial \vec{n}} = 0$ is used on the other boundary edges. Let $\omega_{ei} = 10, \omega_{er} = 100, c_{ve} = c_{vi} = c_{vr} = 1.0$, and there is no source. The time step τ is chosen to be 1.0×10^{-3}. We use the random distorted quadrilateral meshes with the perturbation coefficient being 0.7. See Figure 6, left; the right figure shows the amplified mesh-cells in a local region.

Figure 7 shows the contour of numerical photon temperatures calculated by the NPS (left) and our scheme (right) at $T = 5.0$. The white part in Figure 7 (left) means the numerical values in this region are less than zero.

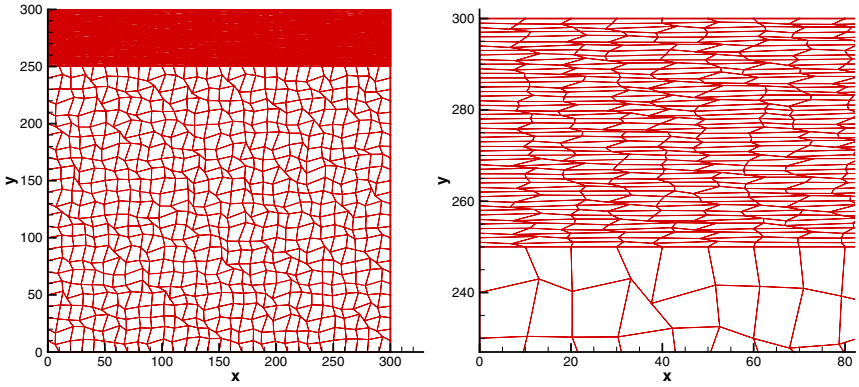

FIG. 6. *The random meshes of Model* 3.

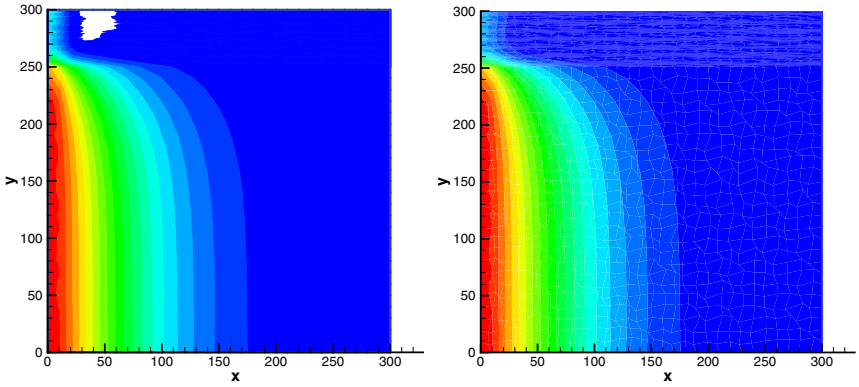

FIG. 7. *The contour of the numerical solutions calculated by the NPS (left) and our scheme (right).*

TABLE 11
The maximum and minimum temperatures of all particles calculated by the NPS for Model 3 *at* $T = 5.0$.

	Electron	Ion	Photon
Maximum	96.336	96.185	96.366
Minimum	-0.510	-0.512	-0.510

TABLE 12
The maximum and minimum temperatures of all particles calculated by our scheme for Model 3 *at* $T = 5.0$.

	Electron	Ion	Photon
Maximum	96.350	96.207	96.379
Minimum	3.0e-4	3.0e-4	3.0e-4

According to the maximum principle of the 3T equations, all the particle temperatures should satisfy the inequality $3.0 \times 10^{-4} \leq u_\alpha(x,t) \leq 100, x \in \Omega, t \geq 0$. Tables 11 and 12 give the maximum and minimum temperatures of all particles calculated by the NPS and our scheme at $T = 5.0$, respectively.

Figure 8 shows the curves of the minimum temperatures for electron, ion, and photon with respect to time, where the lines labeled by NPS_min_e, NPS_min_i,

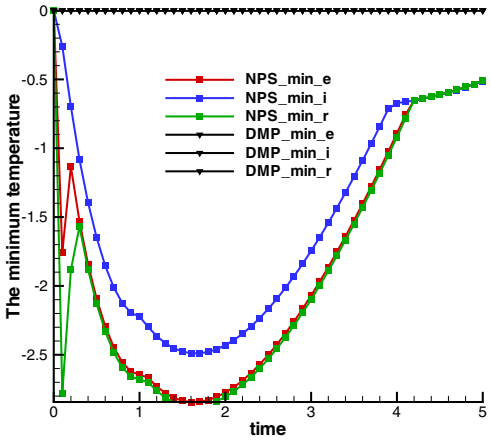

FIG. 8. *The curves of the minimum temperatures of all particle with time.*

TABLE 13
The average number of Picard iterations and used time by our scheme and NPS for Model 3.

Scheme	$it^\sharp$	Used time(s)
Our scheme	4.9	5501.1
NPS	4.3	2665.2

NPS_min_r are the results calculated by the NPS, and the lines labeled by DMP_min_e, DMP_min_i, DMP_min_r are those calculated by our scheme. We can see that all the particle temperatures calculated by our scheme lie in the interval $[3.0 \times 10^{-4}, 100]$, which verifies that our scheme satisfies the DMP. However, the minimum temperatures for electron, ion, and photon calculated by the NPS are all less than 3.0×10^{-4}. This means that the NPS violates the DMP.

Table 13 gives the average number of Picard iterations and the used time of our scheme and NPS. We can see that the computation speed of our scheme is slower than that of NPS, which will be our future work.

6. Conclusions. In this paper, we construct a finite volume scheme satisfying the discrete maximum principle for the coupled system of 3T diffusion equations with both of the Neumann boundary and the Dirichlet boundary. In the construction of the scheme, two kinds of combination of single-sided normal fluxes are used. In the case of the Neumann boundary condition, we use a new method to interpolate the auxiliary unknowns on the boundary with the surrounding cell-centered values. The resulting scheme satisfies the discrete maximum principle and is conservative if the nonlinear iteration system is solved exactly. In addition, the existence of a solution for the nonlinear scheme is proved under some natural conditions on the meshes and known data. Numerical tests show that our scheme has second-order accuracy for the solutions and first-order accuracy for the flux. Conservation errors are approximate to the threshold of nonlinear iteration.

REFERENCES

[1] K. N. CHUEH, C. C. CONLEY, AND J. A. SMOLLER, *Positivity invariant regions for systems of nonlinear diffusion equations*, Indiana Univ. Math. J., 26 (1977), pp. 373–392.

[2] J. Smoller, *Shock Wave and Reaction-Diffusion Equations*, 2nd ed., Springer, New York, 1994.
[3] E. Bertolazzi and G. Manzini, *A second-order maximum principle preserving finite volume method for steady convection-diffusion problems*, SIAM J. Numer. Anal., 43 (2005), pp. 2172–2199.
[4] J. Droniou and C. Le Potier, *Construction and convergence study of schemes preserving the elliptic local maximum principle*, SIAM J. Numer. Anal., 49 (2011), pp. 459–490.
[5] Z. Q. Sheng and G. W. Yuan, *The finite volume scheme preserving extremum principle for diffusion equations on polygonal meshes*, J. Comput. Phys., 230 (2011), pp. 2588–2604.
[6] K. Lipnikov, D. Svyatski, and Y. Vassilevski, *Minimal stencil finite volume scheme with the discrete maximum principle*, Russ. J. Numer. Anal. Math. Model., 27 (2012), pp. 369–385.
[7] C. Cances, M. Cathala, and C. Le Potier, *Monotone corrections for generic cell-centered finite volume approximations of anisotropic diffusion equations*, Numer. Math., 125 (2013), pp. 387–417.
[8] C. Le Potier, *Correction non linéaire et principe du maximum pour la discrétisetion d'opérateurs de diffusion avec des schémas volumes finis centrés sur lesmailles*, C. R. Acad. Sci. Paris Ser. I, 348 (2010), pp. 691–695.
[9] C. Le Potier, *A nonlinear second-order in space correction and maximum principle for diffusion operator*. C. R. Acad. Sci. Paris Ser. I, 352 (2014), pp. 947–952.
[10] J. Droniou, *Finite volume schemes for diffusion equations: Introduction to and review of modern methods*, Math. Models Methods Appl. Sci., 24 (2014), pp. 1575–1619.
[11] Y. Yao and G. Yuan, *Enforcing positivity with conservation for nine-point scheme of nonlinear diffusion equations*, Comput. Methods Appl. Mech. Engrg., 223–224 (2012) pp. 161–172.
[12] G. W. Yuan and Z. Q. Sheng, *Monotone finite volume schemes for diffusion equations on polygonal meshes*, J. Comput. Phys., 227 (2008), 6288–6312.
[13] G. W. Yuan and Y. L. Yu, *Existence of solution of a finite volume scheme preserving maximum principle for diffusion equations*, Numer. Methods Partial Differential Equations, 34 (2018), pp. 80–96 https://doi.org/10.1002/num.22184.
[14] Z. Q. Sheng, J. Y. Yue, and G. W. Yuan, *Monotone finite volume schemes of nonequilibrium radiation diffusion equations on distorted meshes*, SIAM J. Sci. Comput., 31 (2009), pp. 2915–2934.
[15] J. Y. Yue and G. W. Yuan, *Picard-Newton iterative method with time step control for multimaterial non-equilibrium radiation diffusion problem*, Commun. Comput. Phys., 10 (2011), pp. 844–866.
[16] Z. Y. Huang and Y. Li, *Monotone finite point method for non-equilibrium radiation diffusion equations*, Numer. Math., 56 (2016), pp. 659–679.
[17] C. D. Sijoy and S. Chaturvedi, TRHD: *Three-temperature radiation-hydrodynamics code with an implicit non-equilibrium radiation transport using a cell-centered monotonic finite volume scheme on unstructured-grids*, Commun. Comput. Phys., 190 (2015), pp. 98–119.
[18] C. D. Sijoy and S. Chaturvedi, *Combining node-centered parallel radiation transport and higher-order multi-material cell-centered hydrodynamics methods in three-temperature radiation hydrodynamics code TRHD*, Commun. Comput. Phys., 203 (2016), pp. 94–109.
[19] O. Taussky, *Bounds for characteristic roots of matrices*, Duke Math. J., 15 (1948), pp. 1043–1044.
[20] S. Wang, X. D. Hang, and G. W. Yuan, *A pyramid scheme for three-dimensional diffusion equations on general polyhedral meshes*, J. Comput. Phys., 350 (2017), pp. 590–606.
[21] S. Wang, X. D. Hang, and G. W. Yuan, *A positivity-preserving pyramid scheme for three-dimensional diffusion equations on general hexahedral cells with nonplanar faces*, J. Comput. Phys., 371 (2018), pp. 152–167.